to stimulate an appropriate immune response at the site involved in the earliest stages of viral infection.

REFERENCES AND NOTES

1. D. D. Ho *et al*., *Nature* **373**, 123 (1995); X. Wei *et al*., *ibid.*, p. 117; A. Amadori, R. Zamarchi, L. Chieco-Bianchi, *Immunol. Today* **17**, 414 (1996).
2. T. T. MacDonald and J. Spencer, in *Gastrointestinal and Hepatic Immunology*, R. H. Heatley, Ed. (Cambridge Univ. Press, Cambridge, 1994), pp. 1–23.
3. N. Cerf-Bensussan and D. Guy-Grand, *Gastroenterol. Clin. N. Am.* **20**, 549 (1991); J.-P. Kraehenbuhl and M. R. Neutra, *Physiol. Rev.* **72**, 853 (1992).
4. M. Zeitz, W. C. Greene, N. J. Peffer, S. P. James, *Gastroenterology* **94**, 647 (1988); H. L. Schieferdecker, R. Ullrich, H. Hirseland, M. Zeitz, *J. Immunol.* **149**, 2816 (1992).
5. T. Schneider *et al*., *Clin. Exp. Immunol.* **94**, 430 (1994).
6. R. S. Veazey *et al*., *Clin. Immunol. Immunopathol.* **82**, 230 (1997).
7. J. S. McDougal *et al*., *J. Immunol.* **135**, 3151 (1985); G. Nabel and D. Baltimore, *Nature* **326**, 711 (1987); C. J. Van Noesel *et al*., *J. Clin. Invest.* **86** (1990); S. M. Schnittman *et al*., *Proc. Natl. Acad. Sci. U.S.A.* **87**, 6058 (1990); Z. F. Rosenberg and A. S. Fauci, *FASEB J.* **5**, 2382 (1991).
8. R. C. Desrosiers and D. J. Ringler, *Intervirology* **30**, 301 (1989); R. C. Desrosiers, *Annu. Rev. Immunol.* **8**, 557 (1990); K. A. Reimann *et al*., *J. Virol.* **68**, 2362 (1994); A. A. Lackner, *Curr. Top. Microbiol. Immunol.* **188**, 35 (1994).
9. In separate experiments, groups (n = 8) of juvenile (age 1 to 1.5 years) male rhesus macaques were intravenously inoculated with equal doses (50 ng of p27) of molecularly cloned SIVmac239, SIVmac239/316 (a weakly pathogenic, macrophage-competent molecular clone derived from SIVmac239), or SIVmac239Δ*nef* (an attenuated virus derived from SIVmac239 by deleting a large portion of the *nef* gene). Four age- and sex-matched, uninfected macaques were used as controls. All animals were maintained in accordance with the standards of the American Association for Accreditation of Laboratory Animal Care and the guidelines of the Committee on Animals of Harvard Medical School.
10. H. Kestler *et al*., *Science* **248**, 1109 (1990).
11. K. Mori, D. J. Ringler, T. Kodama, R. C. Desrosiers, *J. Virol.* **66**, 2067 (1992).
12. H. W. Kestler *et al*., *Cell* **65**, 651 (1991).
13. Lymphocytes were isolated from the intestinal epithelium, lamina propria, spleen, lymph nodes, and blood and stained for flow cytometric analysis as described (*6*). Samples were stained with monoclonal antibodies (mAbs) to human CD4 (Ortho Diagnostics), CD8, CD25, CD45RA (Becton Dickinson), and rhesus CD3 [T. Kawai *et al*., *Transplant. Proc.* **26**, 1845 (1994)] directly conjugated to fluorescein isothiocyanate, phycoerythrin, peridinin chlorophyll protein, or allophycocyanin. Samples were analyzed using either a FACScan or Vantage flow cytometer and Cell Quest software (Becton Dickinson).
14. R. S. Veazey *et al*., data not shown.
15. In situ hybridization for SIV and immunohistochemistry for macrophages (HAM-56, Dako), CD3, and CD4 were performed on intestinal tissues, peripheral lymph nodes, and spleen as described [C. J. Horvath *et al*., *J. Leukocyte Biol*. **53**, 532 (1993); P. Ilyinskii *et al*., *J. Virol*. **68**, 5933 (1994); J. H. Lane *et al*., *Am. J. Pathol*. **149**, 1097 (1996)]. Absolute numbers of $CD3^+$ T cells were quantitated per square micrometer of intestinal lamina propria by computer-assisted image analysis, as described (*6*). Only LPLs were quantitated because of the technical difficulties involved in discriminating positive cells in Peyer's patches and lymphoid follicles.
16. Statistical analyses were accomplished by means of a Kruskal-Wallis one-way analysis of variance using commercial computer software (Sigma Plot, Jandel). Analyses were performed by comparing the percentages of $CD4^+$ cells of all lamina propria samples (three per animal; jejunum, ileum, and colon) from uninfected normal (n = 12), SIVmac239-infected (n = 6), and SIVmac239Δ*nef*-infected (n = 6) macaques.
17. S. G. Lim *et al*., *Clin. Exp. Immunol.* **92**, 448 (1993); M. Schrappe-Bacher *et al*., *J. Acquired Immune Defic. Syndr. Hum. Retrovirol.* **3**, 238 (1990); T. Schneider *et al*., *Gut* **37**, 524 (1995); V. D. Rodgers, R. Fassett, M. F. Kagnoff, *Gastroenterology* **90**, 552 (1986); F. Clayton *et al*., *ibid.* **103**, 919 (1992).
18. F. Clayton, G. Snow, S. Reka, D. P. Kotler, *Clin. Exp. Immunol.* **107**, 288 (1997).
19. V. G. Sasseville *et al*., *Am. J. Pathol*. **149**, 163 (1996).
20. C. Heise, P. Vogel, C. J. Miller, C. H. Halsted, S. Dandekar, *ibid.* **142**, 1759 (1993).

21. We thank K. Toohey and A. Hampson for photographic assistance, J. Wong for rhesus CD3 mAb, and P. Sehgal and the animal care staff at the New England Regional Primate Research Center for their excellent care of the animals. Supported by NIH grants DK50550, AI38559, AI25328, RR07000, and RR00168. A.A.L. is the recipient of an Elizabeth Glaser Scientist Award.

7 November 1997; accepted 20 February 1998

Association of the AP-3 Adaptor Complex with Clathrin

Esteban C. Dell'Angelica, Judith Klumperman, Willem Stoorvogel, Juan S. Bonifacino*

A heterotetrameric complex termed AP-3 is involved in signal-mediated protein sorting to endosomal-lysosomal organelles. AP-3 has been proposed to be a component of a nonclathrin coat. In vitro binding assays showed that mammalian AP-3 did associate with clathrin by interaction of the appendage domain of its β3 subunit with the amino-terminal domain of the clathrin heavy chain. The β3 appendage domain contained a conserved consensus motif for clathrin binding. AP-3 colocalized with clathrin in cells as observed by immunofluorescence and immunoelectron microscopy. Thus, AP-3 function in protein sorting may depend on clathrin.

The formation of vesicles for transport between organelles of the endocytic and secretory pathways and the selection of cargo for packaging into those vesicles are mediated by protein coats associated with the cytosolic face of the organelles (*1*). The best characterized coats contain clathrin and protein complexes termed "adaptors" (*2*). Clathrin is a complex of three heavy chains and three light chains that polymerizes to form the scaffold of the coats. The adaptors mediate attachment of clathrin to membranes and recruit integral membrane proteins to the coats. Two clathrin adaptors have been described to date—AP-1 and AP-2, which participate in protein transport to the endosomal-lysosomal system from the trans-Golgi network (TGN) and the plasma membrane, respectively.

Recently, another complex related to AP-1 and AP-2 has been identified. This complex, termed AP-3, is composed of two large subunits (δ and β3A or β3B), a medium-sized subunit (μ3A or μ3B), and a small subunit (σ3A or σ3B) (*3*–*8*). AP-3 has been localized to the TGN and endosomes (*4*, *5*) and is involved in protein trafficking to lysosomes or specialized endosomal-lysosomal organelles such as pigment granules, melanosomes, and platelet dense granules (*8*, *9*). Previous studies suggested that AP-3 is a component of a nonclathrin coat (*3*, *4*). However, a critical question has remained unanswered: does AP-3 assemble with a structural coat protein that plays the role of clathrin?

We used glutathione S-transferase (GST) fusion proteins bearing the H (hinge) and C (COOH-terminal) segments of the "appendage" region of human β3A (*6*) to search for this putative protein (Fig. 1A). The reason for selection of these constructs was that both AP-1 and AP-2 bind clathrin via the appendage regions of the β1 and β2 subunits (*10*, *11*). Affinity purification from a cytosolic extract of a human T cell line, Jurkat, resulted in isolation of a prominent 180-kD protein on GST-$\beta3A_C$ but not GST-$\beta3A_H$ or GST columns (Fig. 1B). Unexpectedly, microsequencing of eight tryptic peptides derived from the 180-kD protein identified it as the clathrin heavy chain (Fig. 1B) (*12*). Binding of clathrin to GST-$\beta3A_C$ could also be demonstrated by immunoblotting with antibodies to either the heavy (Fig. 1C, IB, and Fig. 1D, TD.1) or light (Fig. 1D, CON.1) chain of clathrin as well as by immunoprecipitation of metabolically labeled proteins (Fig. 1C, IP). Furthermore, the extent of clathrin binding to GST-$\beta3A_C$ was comparable to that of a GST fusion protein having the

E. C. Dell'Angelica and J. S. Bonifacino, Cell Biology and Metabolism Branch, National Institute of Child Health and Human Development, National Institutes of Health, Bethesda, MD 20892, USA.
J. Klumperman and W. Stoorvogel, Department of Cell Biology, School of Medicine, Institute of Biomembranes, Utrecht University, 3584 CX Utrecht, The Netherlands.

*To whom correspondence should be addressed. E-mail: juan@helix.nih.gov

appendage region of β2 (Fig. 1D, GST-$\beta2_{592–951}$).

The region of β3A that binds clathrin was further delineated by using additional GST-β3A constructs (Fig. 1A). Deletion of the first 19 or 76 residues from the C domain of β3A (GST-$\beta3A_{829–1094}$ or GST-$\beta3A_{886–1094}$) abrogated interaction with clathrin (Fig. 1E, upper). Moreover, a construct having only residues 810 to 885 of β3A was able to bind clathrin. We also analyzed the interaction of the neuronal-specific β3B subunit (*3*) with clathrin. As observed for β3A, the C domain, but not the H domain, of β3B interacted with clathrin (Fig. 1E, upper).

Comparison of amino acids 810 to 885 of β3A to the corresponding segment in β3B revealed three clusters of conserved residues (Fig. 2A). Groups of three or four residues within the clusters were mutated en bloc to alanine residues in the context of the GST-$\beta3A_C$ construct. Mutations of the sequences $SLL^{817–819}$ and $DLD^{820–822}$ within the first cluster (*13*) led to a dramatic decrease in clathrin binding, whereas other mutations had partial ($DFN^{823–825}$) or no effect ($PVS^{826–828}$, $DLE^{845–847}$, $LHL^{849–851}$, $LLHR^{873–876}$) (Fig. 2A) (*14*). Thus, the segment $SLLDLDDFN^{817–825}$ of β3A contained residues that were involved in clathrin binding. Similar amino acid sequences were found within the clathrin-binding regions of β1 and β2 (*11*) as well as within segments of arrestin3 (*15*) and amphiphysin II (*16*) that have been demonstrated to mediate interaction with clathrin (Fig. 2B). Alignment of these sequences defined a consensus motif for clathrin binding that consisted of acidic and bulky hydrophobic residues and conformed to the canonical sequence L(L, I)(D, E, N)(L, F)(D, E).

AP-2 and β-arrestin bind to the "terminal domain" at the NH_2-terminus of the clathrin heavy chain (*17*). To test whether this was also the case for β3A and β3B, we analyzed the binding of radiolabeled clathrin terminal domain to various GST-fusion proteins. Like intact clathrin, the terminal domain fragment specifically bound to the C domains of β3A and β3B as well as to residues 810 to 885 of β3A (Fig. 1E).

To investigate whether the complete AP-3 complex interacted with clathrin, we used a coassembly assay in which clathrin cages were formed in the presence of a mixture of AP-1, AP-2, and AP-3 (*18*). We observed coassembly of AP-3 with clathrin cages to an extent comparable to that of AP-1 and AP-2 (Fig. 2C). Control experiments demonstrated that neither of the three adaptors sedimented in the absence of clathrin and that irrelevant proteins such as bovine serum albumin (BSA) and GST did not associate with clathrin cages (Fig. 2C).

Confocal immunofluorescence microscopy analyses revealed localization of AP-3 in a juxtanuclear area as well as in scattered peripheral foci; 82 ± 6% of these peripheral foci coincided with clathrin-containing structures (Fig. 3). This colo-

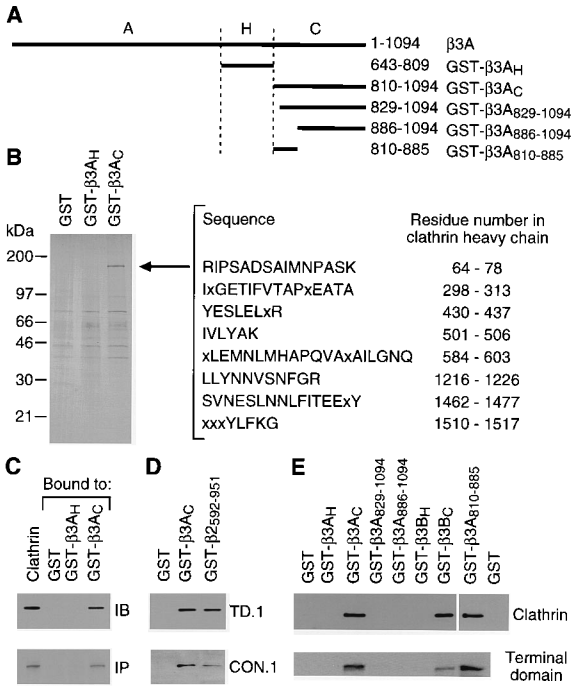

Fig. 1. Interaction of β3A with clathrin. (**A**) Schematic representation of human β3A (*6*) and portions of it expressed as fusions with GST (*20*). (**B**) Isolation of clathrin by affinity chromatography on a GST-$\beta3A_C$ column. Cytosolic proteins that bound to the indicated GST-fusion proteins (*21*) were analyzed by SDS–polyacrylamide gel electrophoresis (SDS-PAGE). Arrow points to a protein that bound only to GST-$\beta3A_C$. The sequences of tryptic peptides derived from this protein matched the segments of clathrin heavy chain indicated in the figure (*12*, *13*). (**C**) Immunoblotting (IB, TD.1 antibody) (*22*) and immunoprecipitation (IP) (*23*) analyses of the binding of clathrin from Jurkat (IB) or HeLa (IP) cytosolic extracts to the indicated GST-fusion proteins. First lane in each panel corresponds to a clathrin-positive control. (**D**) Interaction of clathrin from Jurkat cell cytosol with the clathrin-binding domains of β3A and β2 as analyzed by immunoblotting with antibodies to the heavy (TD.1) or light (CON.1) chains of clathrin (*22*). (**E**) Binding of clathrin from bovine brain cytosol (upper) or [^{35}S]methionine-labeled clathrin terminal domain (*24*) (lower) to GST-fusion proteins bearing portions of β3A or β3B (*20*).

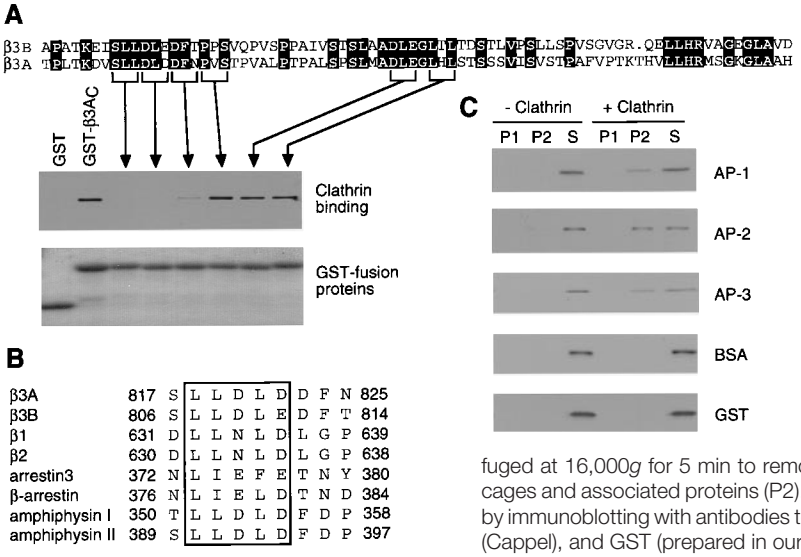

Fig. 2. (**A**) Delineation of a clathrin-binding site within β3A. (Upper) Alignment of residues 810 to 885 of human β3A with residues 799 to 873 of human β3B (*13*). The indicated three-residue groups in the β3A sequence were mutated to alanine triplets in the context of the GST-$\beta3A_C$ construct (*20*). The resulting GST-$\beta3A_C$ mutants, as well as GST and wild-type GST-$\beta3A_C$, were assayed for clathrin binding. (Middle) Immunoblotting of bound proteins from Jurkat cell cytosol with TD.1, the antibody to clathrin. (Lower) SDS-PAGE analysis of GST-fusion proteins. (**B**) Sequence alignment illustrating the existence of a potential clathrin-binding motif within residues 817 to 825 of human β3A and segments of human β3B, β1, and β2; bovine arrestin3 and β-arrestin; and human amphiphysins I and II. (**C**) Coassembly of adaptors with clathrin. A mixture of AP-1, AP-2, and AP-3, containing BSA and GST as irrelevant control proteins, was combined with purified clathrin and dialyzed against a buffer that promotes clathrin cage formation (*18*). Samples without clathrin were processed as controls. Samples were sequentially centrifuged at 16,000*g* for 5 min to remove aggregates (P1) and at 350,000*g* for 10 min to collect clathrin cages and associated proteins (P2). Both P1 and P2 pellets and the final supernatant (S) were analyzed by immunoblotting with antibodies to AP-1 (100/3; Sigma), AP-2 (100/2; Sigma), AP-3 (anti-μ3) (*5*), BSA (Cappel), and GST (prepared in our laboratory).

calization was not likely due to random overlap because in many cases the same "constellations" of foci were recognizable for both AP-3 and clathrin (Fig. 3, insets). In contrast, the overlap of AP-3 with AP-2 amounted to only 12 ± 3% (*14*). Immunoelectron microscopy of thin cryosections revealed the presence of both AP-3 (15-nm gold particles) and clathrin (10-nm gold particles) on tubulovesicular membranes in the proximity of the Golgi stack (Fig. 4A, arrowheads); labeling for AP-3 was also observed on clathrin-positive vacuolar structures reminiscent of endosomes (*14*). The percentage of AP-3–containing membranes that were also labeled for clathrin was 65 ± 5%. To ascertain whether AP-3 colocalized with clathrin on endosomes, we used a whole-mount immunoelectron microscopy technique that allows selective visualization of endosomes loaded with horseradish peroxidase–conjugated transferrin (*19*). We observed colocalization of AP-3 (10-nm gold particles) and clathrin (5-nm gold particles) on 60-nm-diameter buds at the ends of endosomal tubules (Fig. 4B, arrowheads) and, sporadically, on the vacuolar part of endosomes (*14*).

In conclusion, our observations demonstrated an association of the mammalian AP-3 complex with clathrin both in vitro and within cells. This association was mediated by interaction of the C domain of β3(A or B) with the terminal domain of the clathrin heavy chain. Residues in β3 that were involved in this interaction conformed to a consensus motif shared with β1, β2, nonvisual arrestins, and amphiphysins; conservation of this motif is likely to account for the ability of all these proteins to bind clathrin despite their structural diversity. Our findings imply that mammalian AP-3 is likely to function as a clathrin adaptor, just like AP-1 and AP-2. Thus, protein sorting events mediated by AP-3 may also depend on clathrin.

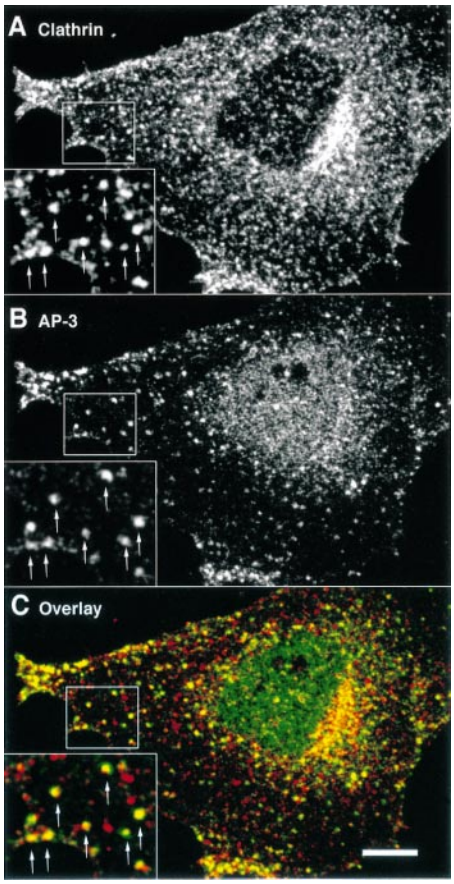

Fig. 3. Confocal immunofluorescence microscopy analysis of colocalization of AP-3 with clathrin. Human HeLa cells were double-stained (*5*) for clathrin [X22 antibody followed by Cy3-conjugated anti-mouse immunoglobulin G; Jackson ImmunoResearch] (**A**) and AP-3 [β3C1 antibody (*6*) followed by Cy2-conjugated anti-rabbit immunoglobulin G; Jackson ImmunoResearch] (**B**). (**C**) Overlay of the images obtained for clathrin (red) and AP-3 (green); yellow indicates colocalization. Insets are magnified views of the smaller rectangular areas of the cytoplasm. Arrows point to structures where clathrin and AP-3 colocalize. Similar results were obtained with antibodies to other AP-3 subunits (*14*). Bar, 10 μm.

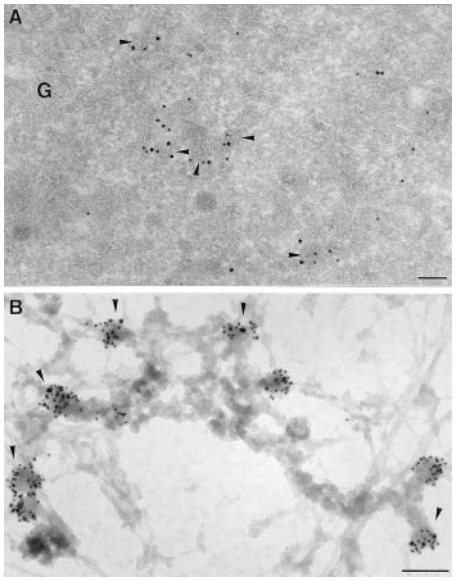

Fig. 4. Immunoelectron microscopy analysis of the colocalization of AP-3 with clathrin. (**A**) Ultrathin cryosections of rat PC12 cells were double-labeled for AP-3 (β3A1 antibody) (*6*) (15-nm gold particles) and clathrin (polyclonal antibody provided by E. Ungewickell) (10-nm gold particles) as described (*25*). Arrowheads point to membranes displaying labeling for both AP-3 and clathrin. G, Golgi stack. (**B**) Human A431 cells were allowed to endocytose transferrin conjugated to horseradish peroxidase (*19*). After the peroxidase reaction, cells were permeabilized, immunolabeled for AP-3 (β3A1 antibody) (10-nm gold particles) and clathrin (X22 antibody) (5-nm gold particles), and examined by whole-mount transmission electron microscopy (*19*). Bars, 100 nm.

REFERENCES AND NOTES

1. J. E. Rothman and F. T. Wieland, *Science* **272**, 227 (1996); R. Schekman and L. Orci, *ibid.* **271**, 1526 (1996).
2. F. M. Brodsky, *Trends Cell Biol.* **7**, 175 (1997); S. L. Schmid, *Annu. Rev. Biochem.* **66**, 511 (1997).
3. L. S. Newman, M. O. McKeever, H. J. Okano, R. B. Darnell, *Cell* **82**, 773 (1995).
4. F. Simpson *et al.*, *J. Cell Biol.* **133**, 749 (1996); F. Simpson, A. A. Peden, L. Christopoulou, M. S. Robinson, *ibid.* **137**, 835 (1997).
5. E. C. Dell'Angelica *et al.*, *EMBO J.* **16**, 917 (1997).
6. E. C. Dell'Angelica, C. E. Ooi, J. S. Bonifacino, *J. Biol. Chem.* **272**, 15078 (1997).
7. H. R. Panek *et al.*, *EMBO J.* **16**, 4194 (1997).
8. C. E. Ooi *et al.*, *ibid*., p. 4508; C. R. Cowles, G. Odorizzi, G. S. Payne, S. D. Emr, *Cell* **91**, 109 (1997).
9. J. D. Stepp, K. Huang, S. K. Lemmon, *J. Cell Biol.* **139**, 1761 (1997); A. B. Seymour *et al.*, *Mol. Biol. Cell* **8**, 227a (abstr.) (1997).
10. S. Schröder and E. Ungewickell, *J. Biol. Chem.* **266**, 7910 (1991); L. M. Traub, S. Kornfeld, E. Ungewickell, *ibid.* **270**, 4933 (1995).
11. W. Shih, A. Gallusser, T. Kirchhausen, *ibid*., p. 31083.
12. Peptide sequences matched segments of clathrin heavy chain encoded on human chromosome 17 (GenBank accession no. D21260) and all but the sequence IVLYAK (*13*) were distinct from those of a homolog encoded on human chromosome 22 (GenBank accession no. X95486).
13. Single-letter abbreviations for amino acid residues are as follows: A, Ala; C, Cys; D, Asp; E, Glu; F, Phe; G, Gly; H, His; I, Ile; K, Lys; L, Leu; M, Met; N, Asn; P, Pro; Q, Gln; R, Arg; S, Ser; T, Thr; V, Val; W, Trp; and Y, Tyr.
14. E. C. Dell'Angelica, J. Klumperman, W. Stoorvogel, J. S. Bonifacino, unpublished observations.
15. J. G. Krupnick, O. B. Goodman Jr., J. H. Keen, J. L. Benovic, *J. Biol. Chem*. **272**, 15011 (1997).
16. A. R. Ramjaun and P. S. McPherson, *Mol. Biol. Cell* **8**, 93a (abstr.) (1997).
17. G. P. Vigers, R. A. Crowther, B. M. Pearse, *EMBO J.* **5**, 2079 (1986); O. B. Goodman Jr., J. G. Krupnick, V. V. Gurevich, J. L. Benovic, J. H. Keen, *J. Biol. Chem.* **272**, 15017 (1997).
18. Clathrin was purified from bovine brain as described by K. Prasad and J. H. Keen [*Biochemistry* **30**, 5590 (1991)]. To obtain a protein fraction enriched in AP-1, AP-2, and AP-3, we extracted total bovine brain membranes overnight with extraction buffer [0.5 M tris-HCl (pH 7.5), 2 mM dithiothreitol, 1 mM EDTA, 3 mM NaN_3]. The extracted proteins were concentrated by ammonium sulfate precipitation and fractionated on a Superose 6 column (2.5 × 45 cm) equilibrated with extraction buffer. Fractions containing the adaptors (elution volume, 120 to 135 ml) were pooled. For the coassembly assay, the adaptor pool (40 μg of protein) was combined with purified clathrin (40 μg) and control proteins (BSA and GST, 10 μg each) in 0.2 ml of extraction buffer, and the mixture was dialyzed against 0.1 M potassium tartrate, 10 mM Hepes (pH 7.0), 1 mM EGTA, 2 mM dithiothreitol, 0.8 mM 4-(2-aminoethyl)-benzenesulfonyl fluoride, and 0.5 mM $MgCl_2$ for 12 to 14 hours at 4°C.
19. W. Stoorvogel, V. Oorschot, H. J. Geuze, *J. Cell Biol.* **132**, 21 (1996).
20. Preparation of GST-fusion proteins bearing residues 643 to 809 and 810 to 1094 of β3A and residues 647 to 796 of β3B (GST-$\beta3A_H$, GST-$\beta3A_C$ and GST-$\beta3B_H$, respectively) has been described (*5*, *6*). The following GST-fusion constructs were generated by polymerase chain reaction (PCR) amplification and cloning into the Eco RI–Not I sites of the pGEX-5X-1 vector (Pharmacia Biotech): GST-$\beta3B_C$ (residues 799 to 1081 of β3B), GST-$\beta3A_{829-1094}$, GST-$\beta3A_{886-1094}$, and GST-$\beta2_{592-951}$. The GST-$\beta3A_{810-885}$ construct was obtained by site-directed mutagenesis of GST-$\beta3A_C$ to introduce a stop codon at position 886 of β3A.
21. A cytosolic extract from Jurkat cells was passed through columns of GST, GST-$\beta3A_H$, or GST-$\beta3A_C$ coupled to Affi-Gel 15 (Bio-Rad). Bound proteins

were washed with 0.1% (w/v) saponin in phosphate-buffered saline and then eluted with 0.1 M glycine (pH 2.5).
22. I. S. Näthke *et al.*, *Cell* **68**, 899 (1992).
23. A cytosolic extract from [^{35}S]methionine-labeled HeLa cells (*5*) was incubated with GST, GST-β3A$_H$, or GST-β3A$_C$ coupled to Affi-Gel 15 beads. Bound proteins were eluted by heating the beads at 95°C for 5 min in the presence of 1% (w/v) SDS, 10 mM dithiothreitol, 0.1 M tris-HCl (pH 7.4). Samples were diluted 1:20 with 50 mM tris-HCl buffer (pH 7.4) containing 1% (w/v) Triton X-100, 0.3 M NaCl, 10 mM iodoacetamide, 5 mM EDTA, 0.1% (w/v) BSA and immunoprecipitated (*5*) with the X22 antibody [F. M. Brodsky, *J. Cell Biol.* **101**, 2047 (1985)].
24. A cDNA fragment encoding residues 1 to 579 of human clathrin heavy chain was engineered by PCR for cloning into the Bam HI–Xho I sites of the pBluescript SK II vector (Stratagene). In vitro transcription-translation was performed in the presence of [^{35}S]methionine using the TNT system (Promega). The translated products were diluted 1:10 in 50 mM Hepes buffer (pH 7.4) containing 0.1 M KCl, 2 mM $MgCl_2$, 0.1 mM $CaCl_2$, 10% (v/v) glycerol, 0.1% (w/v) BSA, and 0.05% (w/v) Triton X-100 and centrifuged at 120,000*g* for 30 min at 4°C to remove protein aggregates.
25. J. W. Slot, H. J. Geuze, Gigengack, S., G. E. Lienhard, D. E. James, *J. Cell Biol.* **113**, 123 (1991).
26. We thank M.-C. Fournier and V. Oorschot for excellent technical assistance; L. Green and E. Eisenberg for advice on the purification of clathrin; F. Brodsky, L. Samelson, E. Ungewickell, and W. Zhang for generous gifts of reagents; and J. Donaldson, J. Lippincott-Schwartz, C. E. Ooi, and G. Storz for critical review of the manuscript.

12 December 1997; accepted 17 February 1998

NMR Structure of a Classical Pseudoknot: Interplay of Single- and Double-Stranded RNA

Michaël H. Kolk, Marinette van der Graaf,* Sybren S. Wijmenga,† Cornelis W. A. Pleij,‡ Hans A. Heus, Cornelis W. Hilbers§

Pseudoknot formation folds the 3′ ends of many plant viral genomic RNAs into structures that resemble transfer RNA in global folding and in their reactivity to transfer RNA–specific proteins. The solution structure of the pseudoknotted T arm and acceptor arm of the transfer RNA–like structure of turnip yellow mosaic virus (TYMV) was determined by nuclear magnetic resonance (NMR) spectroscopy. The molecule is stabilized by the hairpin formed by the 5′ end of the RNA, and by the intricate interactions related to the loops of the pseudoknot. Loop 1 spans the major groove of the helix with only two of its four nucleotides. Loop 2, which crosses the minor groove, interacts closely with its opposing helix, in particular through hydrogen bonds with a highly conserved adenine. The structure resulting from this interaction between the minor groove and single-stranded RNA at helical junctions displays internal mobility, which may be a general feature of RNA pseudoknots that regulates their interaction with proteins or other RNA molecules.

RNA pseudoknots are found in virtually all classes of RNA and play key roles in a variety of biological processes. They often constitute a local structural element that may act as a recognition site for proteins involved in replication initiation or translational regulation (*1*). The formation of most functional pseudoknots involves Watson-Crick base pairing of residues in an RNA hairpin loop with nucleotides outside that loop, yielding two stems that are mutually connected by two nonequivalent loops. Stacking of these helical segments is thought to add to the overall stability of the pseudoknot and represents a major feature of the functional pseudoknots described to date (*2*–*4*). Consistent with the RNA A-helical geometry, the connecting loops 1 and 2 are always located on opposite sides of the helix, at the major and minor groove side, respectively; however, detailed information on tertiary structure in the pseudoknot and on the determinants of its stability has not been available.

Here we describe the NMR structure of a pseudoknotted fragment that was resolved at an atomic level in all regions, allowing an accurate description of the interplay of single- and double-stranded regions responsible for the distinct structural and dynamic properties of the molecule. The system matches the complete T arm and valine acceptor arm of the tRNA-like structure of TYMV genomic RNA (Fig. 1A). This structure was the earliest example found of this class of pseudoknot motifs (*5*, *6*), which is present in the genomic RNAs of many plant viruses (*7*). The tRNA mimicry is achieved through pseudoknot formation in the aminoacyl acceptor arm, which leads to a global folding of the entire tRNA-like structure into an L-shaped molecule, despite a secondary structure that is very different from tRNA (*6*, *8*). The structural resemblance to tRNA is also evident from its reactivity to tRNA-specific enzymes, such as cleavage by ribonuclease (RNase) P and aminoacylation by valyl-tRNA synthetase, as in the case of TYMV genomic RNA (*7*, *9*).

The 44-nucleotide RNA molecule we studied is identical to the 3′-terminal region of TYMV RNA, with the exception of some structurally silent alterations in the stem and loop of the hairpin at the 5′ side of the acceptor arm (*10*), which is required to seal down an otherwise unstable pseudoknot (*11*). The size of the molecule required the use of both uniformly and selectively (A-only and U-only) ^{13}C- and ^{15}N-labeled samples for the NMR structure determination (*12*). Selective labeling proved essential for assigning the resonances of loop residues and of residues located near the helical junction sites, some of which are severely broadened (Fig. 1B). We could identify most resonances with standard triple-resonance techniques, but some additional experiments were needed for complete assignment of the sugar-spin systems (*13*). Distance and dihedral restraints derived from the NMR data were used for structure calculations (*14*) to obtain the final ensemble of 10 structures (Table 1 and Fig. 2).

The average structure shows an A-type helical conformation for all three stem regions. Colinearity is maintained at both helical junction sites. Slight torsional and swaying motions between these helices on a millisecond time scale are most likely responsible for the observed line broadening for residues near the interface of stems 1 and 2. Changes in the ring-current effects resulting from even a modest dislocation of an aromatic moiety can result in a significant change in the chemical shift of nearby protons (*15*), even if the latter themselves are within a stable Watson-Crick base pair. This type of dynamics probably also accounts for similar line broadening reported for a different pseudoknot (*3*), and we expect it to be a general phenomenon of this class of RNA motifs.

The rod-shaped molecule is capped by a seven-membered loop that is comparable to the T loop in tRNA. Although two mutations were introduced at the 5′ side of the loop, its sequence contains all the

Nijmegen SON Research Center for Molecular Structure, Design and Synthesis, Laboratory of Biophysical Chemistry, University of Nijmegen, Toernooiveld, 6525 ED Nijmegen, The Netherlands.

*Present address: Department of Radiology, University Hospital Nijmegen, 6500 HB Nijmegen, The Netherlands.
†Present address: Department of Medical Biochemistry and Biophysics, University of Umeå, S901 87, Sweden.
‡Present address: Leiden Institute of Chemistry, University of Leiden, 2300 RA Leiden, The Netherlands.
§To whom correspondence should be addressed.